AAS 18-381

EARLY TRAJECTORY ESTIMATE OF PROXIMATE OBJECTS WITH AN OPTICAL FENCE

**Liam M. Healy, Scott Kindl, Christopher R. Binz,
Christoph Englert, Andrew Nicholas
Naval Research Laboratory
Washington, DC 20375**

An on-board optical fence using a light sheet and camera provides angles-only relative orbital knowledge of objects in its vicinity and can be used to make early estimates of the relative orbit, before anything else is known about it. The dwell time that the secondary spends in the vicinity of the sensor host with the light sheet perpendicular to the direction of motion can be estimated from three detections, that is, crossings of the sheet. With two parallel and closely spaced sheets, the complete two-dimensional relative motion in the host's orbital plane can be determined.

INTRODUCTION

The ability to detect and track objects in close proximity to a spacecraft is important for safe operations in a crowded orbital environment. Ground-based sensor resolution limits the apparent distance at which two objects may be reliably distinguished and tracked, meaning a local situational awareness capability becomes beneficial for providing accurate knowledge of the relative states between the two objects [1].

Commercial satellite servicing is close to becoming a reality [2], which could dramatically change the way spacecraft operate in orbit. With an increase in robotic capability in space, regular servicing missions and even in-space assembly become feasible, leading to a sharp rise in the number of missions involving rendezvous and proximity operations. While most concepts assume the servicer has the instrumentation necessary for relative navigation, it may make sense to equip spacecraft with sensors that provide cooperative relative navigation information to the the servicer. In addition, a future in-space assembly site could benefit from local surveillance sensors for operational safety.

A concept developed by Englert et al. [3] for a local, low size, weight and power situational awareness sensor uses a conical mirror that spreads a collimated light beam into a sheet of light, which then scatters off of any object that passes through it. The scattered light is observed by a wide angle detector, resulting in an angular measurement of the position of the object; see fig. 1 for an illustration of this concept. Traditional concepts with visible light cameras depend heavily on favorable light conditions and potentially have limited fields of view. This sensor would provide near-real-time, persistent monitoring of local space, far beyond the limits of ground-based space situational awareness sensors, and without the restrictions on field of view or lighting conditions. A device or multiple such devices could be attached to a spacecraft in a variety of ways. A possible deployment of a single such device on a spacecraft is illustrated in fig. 2.

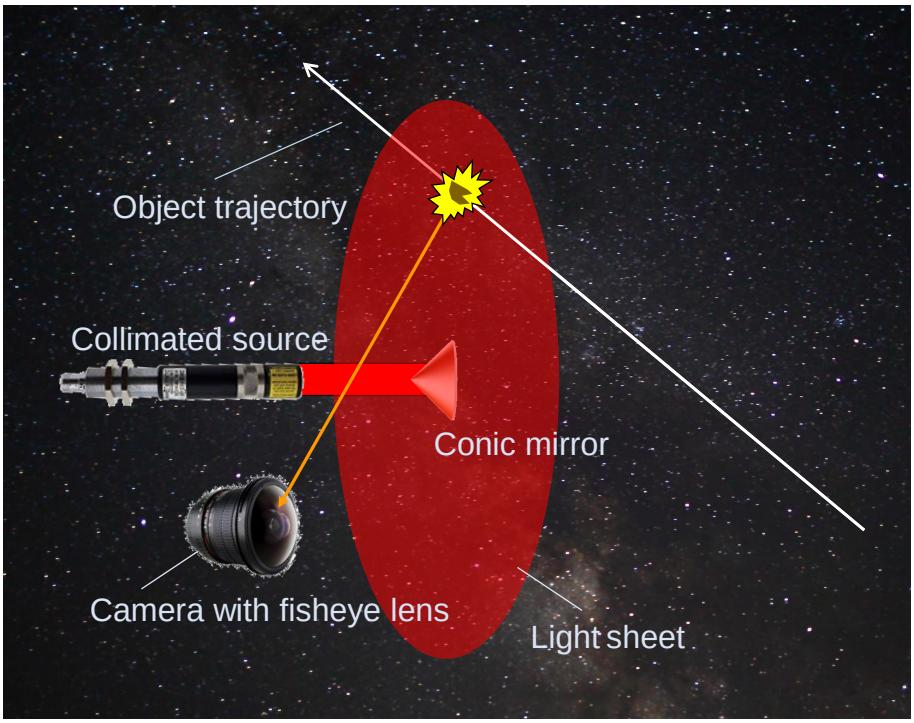

Figure 1: Light sheet detector

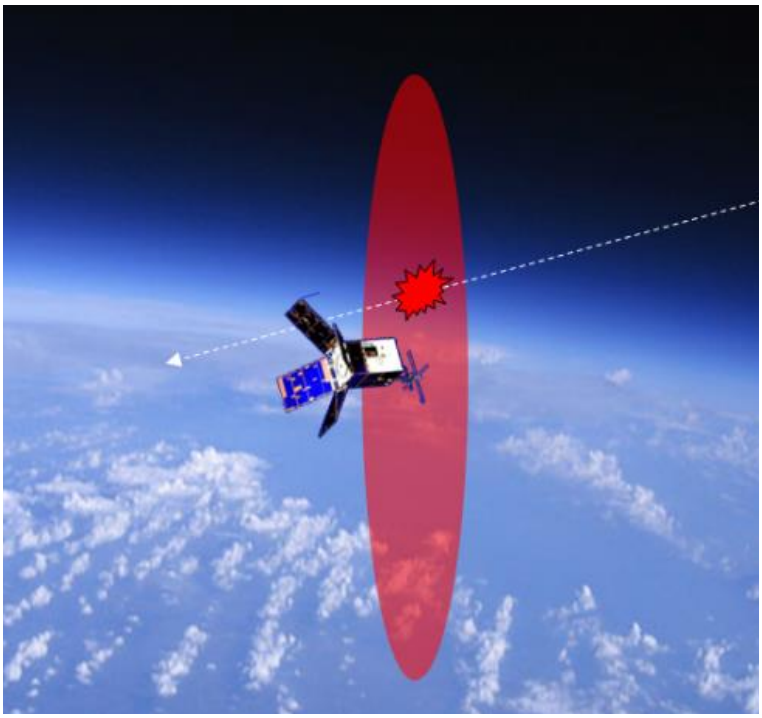

Figure 2: Conceptual diagram of light sheet detector deployment on orbit

The present task is to obtain information about the relative motion of the secondary from only one sheet and sensor with only angle information, and then to expand that with a second sheet. With only one observation point, no maneuvers, no perturbations, and in the linear approximation, the size of the relative orbit is unobservable for an angles-only sensor; see Woffinden and Geller [4]. These authors claim but do not show that a "shape parameter" p, defined as the ratio of the minimum to maximum extreme relative altitudes, is observable. The shape parameter $p = 1$ corresponds to a co-elliptic trajectory, so that the observed object will be seen only once (before the next synodic period). The shape parameter $p = -1$ corresponds to periodic relative motion. Values $|p| > 1$ are possible (contrary to the statement of the authors) and correspond to the secondary object having a smaller semimajor axis than the primary, but qualitatively they are the same as the $1/p$ relative orbits except with the relative direction of motion opposite. With a second sheet, the scale is observable.

Our concept for this sensor is to get an early trajectory estimate of nearby objects that are on periodic or nearly periodic relative trajectories, and thus will be repeatedly observed on a time scale of an orbital period; the transient passage of the secondary on a near-coelliptic orbit is less interesting. Since multiple observations are needed to determine a relative orbit anyway, a single observation would not be sufficient to learn much about the secondary. A relative orbit that is near-periodic and thus repeatedly crosses the sheet can be partially determined. Our interest is in how long it will remain close to the host vehicle. Figure 3 shows various points along the continuum from one observation (crossing of the local vertical plane orthogonal to the direction of motion) to infinitely many. Figure 4 shows a trajectory crossing the vertical plane with plane and crossing points highlighted. In the periodic relative motion case, the time intervals between observations will alternate between two values; in the case illustrated, with the vertical plane at the center of the relative ellipse, all the time intervals are the same.

To simplify the analysis, we assume that the host satellite is in a circular orbit, and ignore relative motion out of the orbital plane. The data from the camera is simply the times at which the object crosses the sheet; it is assumed there is only one secondary and that it does not maneuver.

RELATIVE MOTION

In Healy and Henshaw [5] equations (1a) and (1b), it is shown that in-plane relative motion about a circular orbit can be written as a 2:1 ellipse centered on two constants of motion x_c and y_c, the radial and in-track centers respectively, and drifting in-track

$$x = x_c + \sin\tau, \tag{1a}$$

$$y = y_c - \frac{3}{2}x_c(\tau - \tau_0) + 2\cos\tau, \tag{1b}$$

where the unobservable scale κ has been set to 1 or equivalently, all lengths are in units of κ. The variable τ changes at a constant rate, $\dot{\tau} = n$, the mean motion of the host. The value of τ_0 is unknown and unobservable; $\tau = \tau_0$ corresponds to the point at which $x = x_c$, but as x_c (like y_c) is not known, it is also unknown. For our purposes y_c can be redefined to include the τ_0 term. Therefore, we define

$$\bar{y}_c = y_c + \frac{3}{2}x_c\tau_0 \tag{2}$$

and rewrite eq. (1b)

$$y = \bar{y}_c - \frac{3}{2}x_c\tau + 2\cos\tau. \tag{3}$$

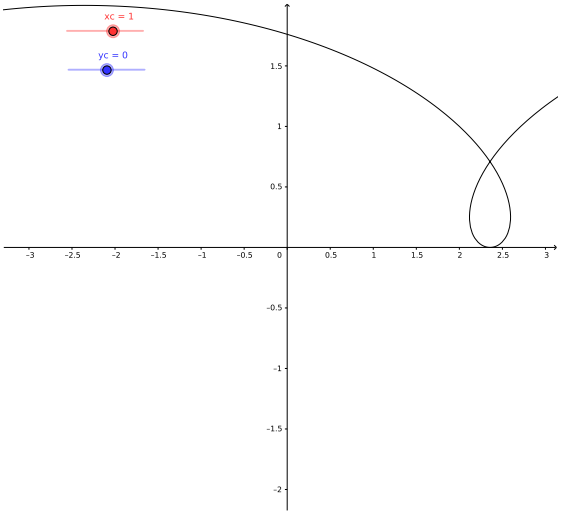

(a) One crossing, $x_c = 1$, $y_c = 0$

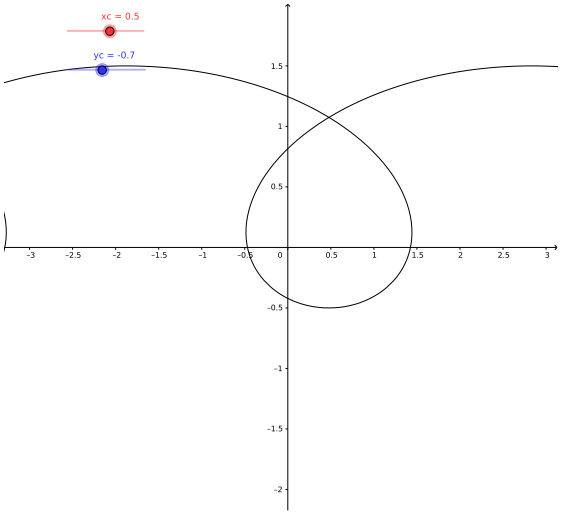

(b) Three crossings, $x_c = 0.5$, $y_c = -0.7$

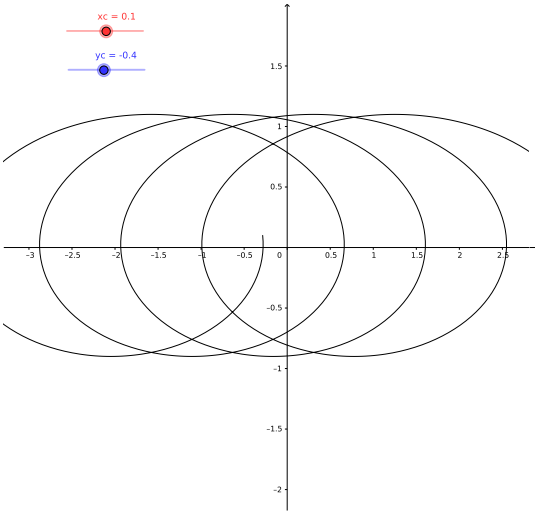

(c) Seven crossings, $x_c = 0.1$, $y_c = -0.4$

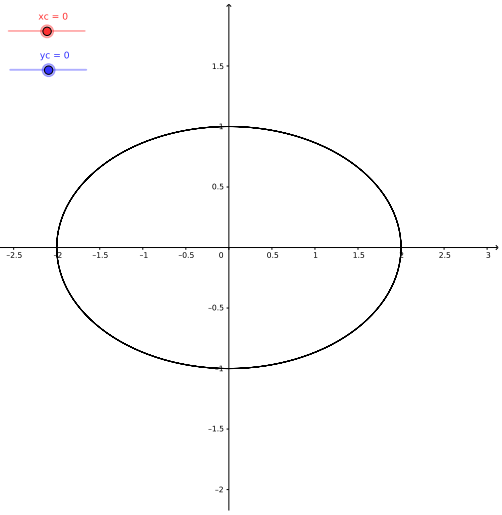

(d) Infinite crossings (periodic), $x_c = 0$, $y_c = 0$

Figure 3: Relative motion for various values of the parameters x_c and y_c; radial direction is up, in-track direction to the left

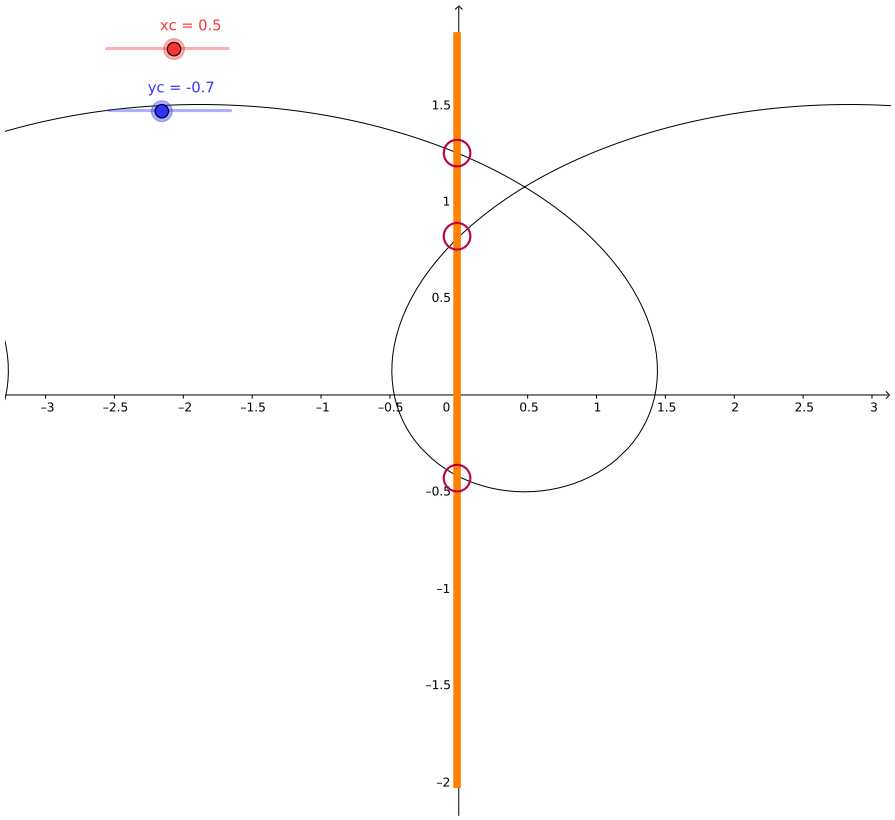

Figure 4: Crossing vertical plane at three times for $x_c = 0.5$, $y_c = -0.7$

The value of x_c can be any real number; the in-plane relative motion is illustrated in fig. 3 for a variety of x_c values. A value of zero represents periodic relative motion (fig. 3d), positive values represent a secondary that has a larger orbital period than the primary and negative values represent one that has a smaller orbital period. For a given x_c, the relative trajectory for its negative looks the same, but reflected about the in-track axis and with the relative direction of motion opposite (positive vbar to negative or vice versa). Co-elliptic trajectories correspond to $x_c = \pm\infty$ in the notation used here because they have zero scale $\kappa = 0$.

A crossing of the vertical plane corresponds to $y = 0$,

$$0 = \bar{y}_c - \frac{3}{2}x_c\tau + 2\cos\tau \tag{4}$$

or

$$\bar{y}_c = \frac{3}{2}x_c\tau - 2\cos\tau. \tag{5}$$

As $|x_c|$ decreases from infinity, there continues to be only one point in the trajectory with a given in-track location. The loops seen in fig. 3 form as $|x_c|$ is decreased when the derivative $\partial\bar{y}_c/\partial\tau$ has one solution per revolution, which happens at $|x_c| = 4/3$. For values $|x_c| < 4/3$, there are loops; once there are loops, there is the possibility of multiple observations.

The relative orbit cannot be determined until there have been three observations of the secondary crossing the plane. The value of τ at the first crossing may be determined from the two later times as follows. Designate the three observation times as τ_1, τ_2, and τ_3. None of these values are known after the measurements, but the differences of the latter two from the first, $s_2 = \tau_2 - \tau_1 = n\Delta t_{12}$ and $s_3 = \tau_3 - \tau_1 = n\Delta t_{13}$ respectively, are known, based on the elapsed times between detections, Δt_{12} and Δt_{13}. We wish to find the value τ_1. Since $\bar{y}_c$ is a constant of motion, by setting the two right-hand sides of eq. (5) equal for $\tau = \tau_1$ and $\tau = \tau_2$, we have

$$x_c = \frac{4}{3}\frac{\cos\tau_1 - \cos\tau_2}{\tau_1 - \tau_2} = \frac{4}{3}\frac{\cos(\tau_1 + s_2) - \cos\tau_1}{s_2}. \tag{6}$$

Notice that the particular value of y (assumed zero here) is not relevant; the only important part is that it is the same for all observations. Physically, this means as long as the sheet is vertical, it can be placed anywhere along the in-track axis of the spacecraft body. Since x_c is a constant, a similar equation is true for points 1 and 3, and we can set these equal and rearrange

$$\frac{s_2}{s_3} = \frac{\cos\tau_1 - \cos(\tau_1 + s_2)}{\cos\tau_1 - \cos(\tau_1 + s_3)} \tag{7}$$

$$= \frac{\cos\tau_1 - \cos\tau_1\cos s_2 + \sin\tau_1\sin s_2}{\cos\tau_1 - \cos\tau_1\cos s_3 + \sin\tau_1\sin s_3} \tag{8}$$

$$= \frac{1 - \cos s_2 + \tan\tau_1\sin s_2}{1 - \cos s_3 + \tan\tau_1\sin s_3} \tag{9}$$

which is a linear equation in, and thus may easily be solved for $\tan\tau_1$,

$$\tan\tau_1 = \frac{s_2(1 - \cos s_3) - s_3(1 - \cos s_2)}{s_3\sin s_2 - s_2\sin s_3}. \tag{10}$$

Note there are multiple values of τ_1 every half revolution that solve this equation. However, from eqs. (5) and (6), it is clear that adding even multiples of π does not change the value of either x_c or $\bar{y}_c$, and adding odd multiples only changes the sign of both. It may be seen in the next section that neither affects the computed times.

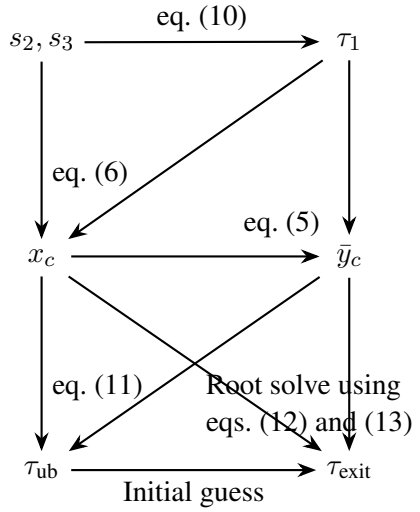

Figure 5: Variable computation of exit time τ_{exit} from observation time intervals s_2, s_3

TIME OF CIRCUMNAVIGATION

The computed x_c can tell us what we will call the *time to circumnavigation exit*, the time until the last vertical plane crossing. If the relative motion is periodic, then this time is infinite.

Once τ_1 is known, substitution in eq. (6) gives x_c. From this, $\bar{y}_c$ may be computed from eq. (5) with the known $\tau_i = \tau_1 + s_i$ for $i = 1, 2$. This allows us to predict all future plane crossings with eq. (16), and in particular, the final crossing of the vertical plane.

If $\frac{3}{2}x_c\tau > 2 + \bar{y}_c$, then there is no solution for any greater τ if $x_c > 0$. Defining the upper bound time τ_{ub} for τ, if

$$\tau > \tau_{\text{ub}} = \frac{4 + 2\bar{y}_c}{3x_c}, \tag{11}$$

there are no further plane crossings. As we expect, there is an x_c in the denominator; $x_c = 0$ corresponds to periodic relative motion and therefore no circumnavigation exit and no upper bound.

From this upper bound, the time of the last plane crossing, τ_{last} can be computed with a root solver as follows. First, the time of second observation τ_2 is computed from s_2 and τ_1 (eq. (10)). Then from the computed x_c and $\bar{y}_c$ (eqs. (5) and (6)), compute the y relative position values in the interval between τ_2 and τ_{ub}. Then search for a change in the sign of the y values starting at τ_{ub}. From the first crossing found, interpolate between the two values and use that as the initial guess for the Newton solver.

A Newton solver is applied with eq. (4) expressed as a function to be nulled,

$$f(\tau) = \bar{y}_c - \frac{3}{2}x_c\tau + 2\cos\tau \tag{12}$$

and its time (τ) derivative

$$f'(\tau) = -\frac{3}{2}x_c - 2\sin\tau \tag{13}$$

to solve for the exact time τ_{last} of circumnavigation exit. Figure 5 is a diagram of variable dependencies and equation references for the complete calculation of the circumnavigation exit time.

As noted in the previous section, adding or (subtracting) odd multiples of π in the computation of τ_1 changes to the sign of x_c and y_c, but it can be seen from this equation that it does not change the resultant computed time. The elapsed time from first observation to exit is then the difference $s_{\text{exit}} = \tau_{\text{last}} - \tau_1$.

In addition to time to circumnavigation exit, it is useful to know the time elapsed since circumnavigation entrance, defined as the time at which the object first crossed the $y = 0$ plane. Time from circumnavigation entrance to the first observation may be computed similarly to how time to exit is computed. First, the time of first observation τ_1 is computed from s_2 and s_3 using eq. (10). Then from the computed x_c and $\bar{y}_c$ (eqs. (5) and (6)), compute the y relative position values in the interval between $-\tau_{\text{ub}}$ and τ_1 using the computed x_c and $\bar{y}_c$. Then search for a change in the sign of the y values starting at the negative upper bound of τ. From the first crossing, interpolate between the two values and use that as a guess for a Newton solver, which when converged, gives τ_{first}. The elapsed time from entrance to first observation is then the difference $s_{\text{enter}} = \tau_1 - \tau_{\text{first}} \geq 0$.

From these quantities, a *total dwell time* can be computed by summing with the time to exit, $\tau_{\text{dwell}} = s_{\text{enter}} + s_{\text{exit}}$. It is measured in radians of the host orbit. It shows the total time the secondary has spends where its relative orbit crosses the selected vertical plane if there are no maneuvers. A longer time indicates that the orbital periods are more closely matched, which is important for docking and other cooperative work.

This computation is subject to uncertainty. The uncertainty can come from numerous sources: timing errors including ambiguity of sheet crossing from observation to observation, uncertainty of the host orbit mean motion, and eccentricity of the host orbit for example.

SCALE WITH TWO SHEETS

While the time to circumnavigation exit is useful information, it is not complete information about the relative orbit; the scale κ is unobservable. However, if there are two parallel sheets close together, this can be computed. From eq. (1e) of Healy and Henshaw [5]

$$\frac{\dot{y}}{\kappa} = -\frac{3}{2} n x_c - 2n \sin \tau, \tag{14}$$

where again x_c here is in units of κ, i.e., scaled by κ relative to the original equation. From knowing the separation of the light sheets and the time to traverse the sheets, we may compute $\dot{y}$ and thus κ. Triangulation, for example, stereoscopic vision, is able to determine distances well within a few multiples of the sensor separation, but with an accuracy that degrades quickly at greater distances. However, that is not the case here, due to the use of orbital mechanics information.

With two parallel vertical sheets separated by a distance d, the scale is found from

$$\kappa = -\frac{d}{n\delta t \left(\frac{3}{2} x_c + 2 \sin \tau_1\right)}, \tag{15}$$

where δt is the time (in seconds) between the sheet crossings when $\tau = \tau_1$ at the first sheet crossing. Uncertainty in determining scale will be due to differential timing errors, profile uncertainty for larger objects, and angular divergence of the sheet at larger distance.

With the determined x_c, $\bar{y}_c$, and κ the complete in-plane relative orbital motion may be solved

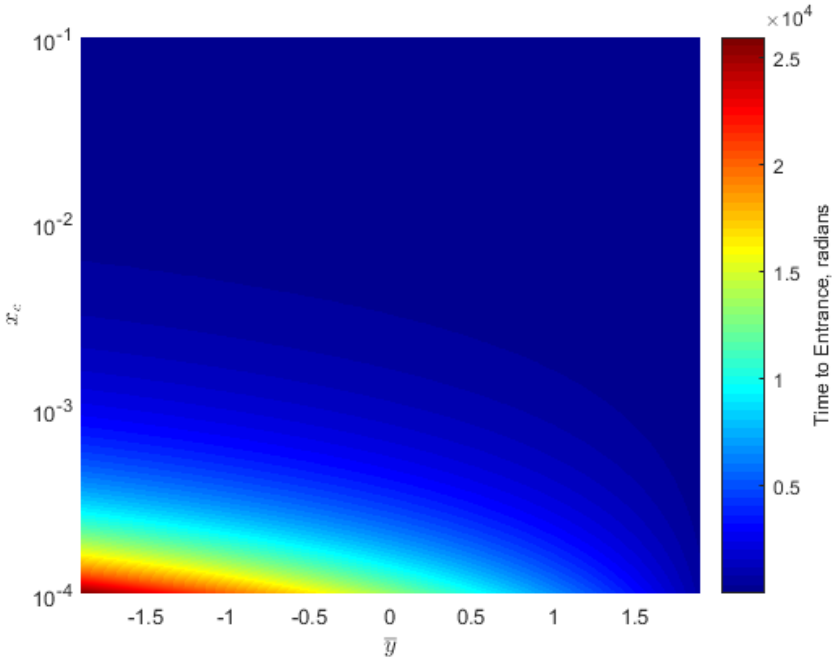

Figure 6: Time from circumnavigation entrance to first observation by x_c and $\bar{y}_c$

using eqs. (1a) and (1b) of [5],

$$x = \kappa[x_c + \sin(\tau_1 + s)] \tag{16}$$

$$y = \kappa[\bar{y}_c + 2\cos(\tau_1 + s)], \tag{17}$$

where s is the elapsed time in radians of the host orbit from the first observation.

RESULTS

To test these algorithms, multiple relative orbits are generated by picking values in the range $0 < x_c < 0.1$, computing resultant relative motion and determining the times between plane crossings. From this data, the times from entrance and to exit is computed from the s_2, s_3 pairs using the process outlined in fig. 5 and described above. The time from circumnavigation entrance, time to exit, and total (dwell) time are shown for a range of simulated x_c and $\bar{y}_c$ in figs. 6 to 8. Note that the dwell time is independent of $\bar{y}_c$, so it has been plotted as dwell time vs. x_c in fig. 9. A power law regression shows that the dwell time in radians is roughly inversely proportional to x_c,

$$\tau_{\text{dwell}} = 2.3105 x_c^{-1.019}, \tag{18}$$

with a coefficient of determination $R^2 = 0.9998$. Thus with the simple formulas eqs. (6), (10) and (18), the dwell time may be computed from the time differences measured.

Errors in the measured values of s_2 and s_3 give rise to errors in the dwell time result. With deliberately introduced errors in the range $\pm 1\,\text{mrad}$ for s_2 and s_3, the percent errors of the dwell time are shown in figs. 10 to 13 for $x_c = 1 \times 10^{-4}$ through $x_c = 0.1$. Interestingly, the error is essentially independent of s_2 error and only dependent on s_3 error. The plots show the average over

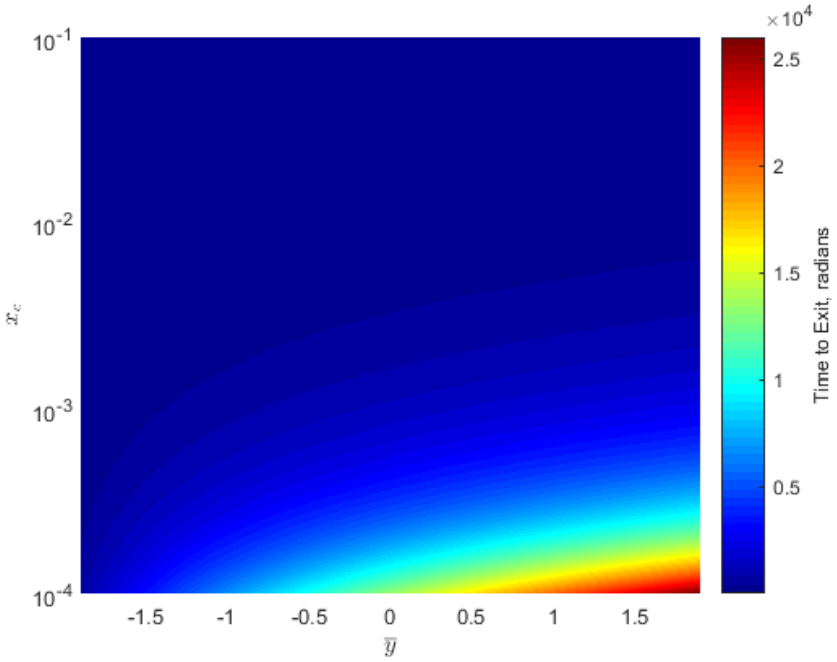

Figure 7: Time from first observation to circumnavigation exit by x_c and $\bar{y}_c$

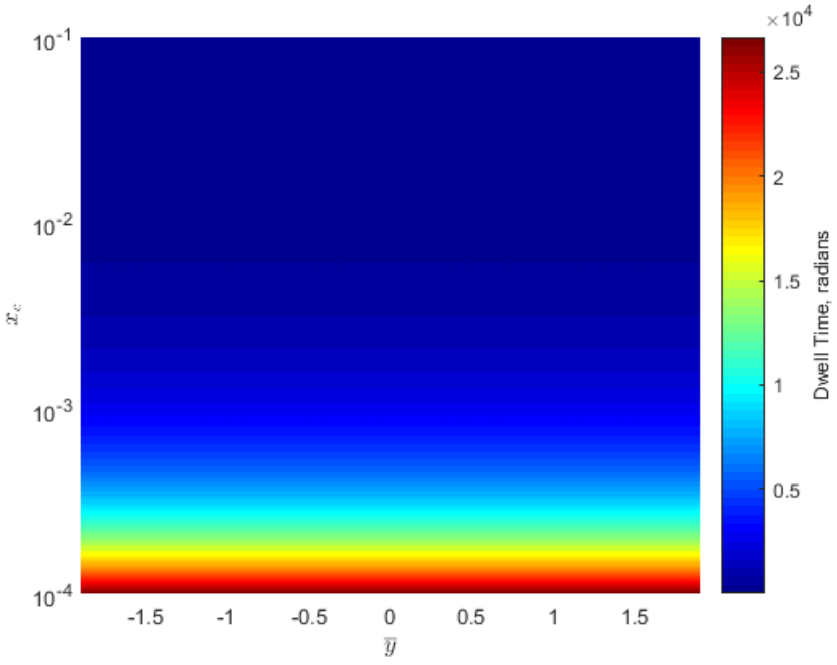

Figure 8: Circumnavigation dwell time by x_c and $\bar{y}_c$

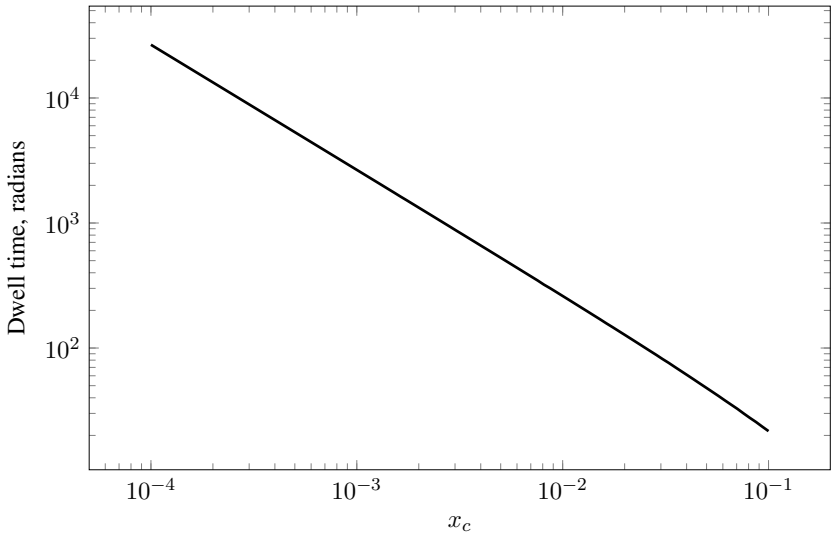

Figure 9: Circumnavigation dwell time by x_c

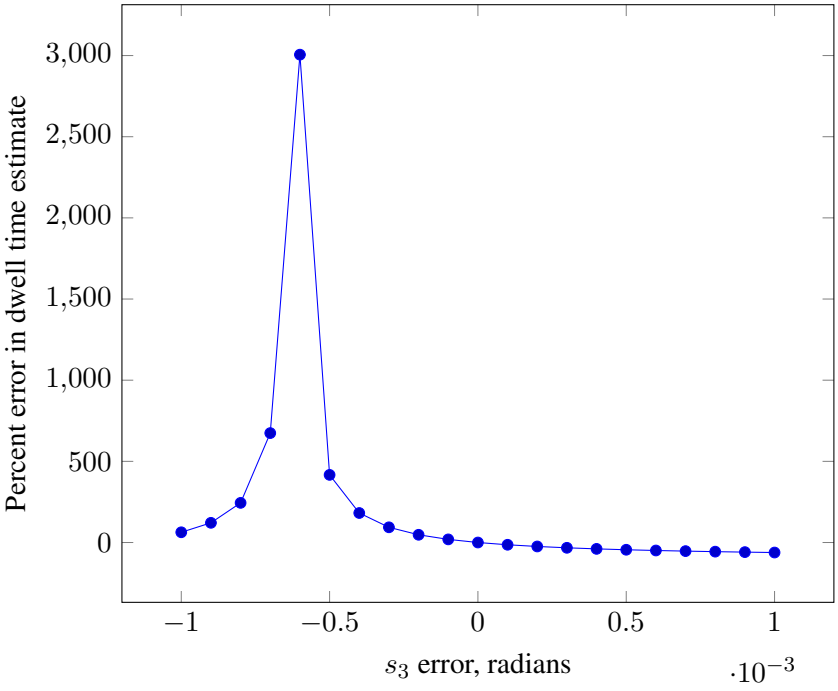

Figure 10: Percent error in dwell time from error in s_3 for $x_c = 0.0001$

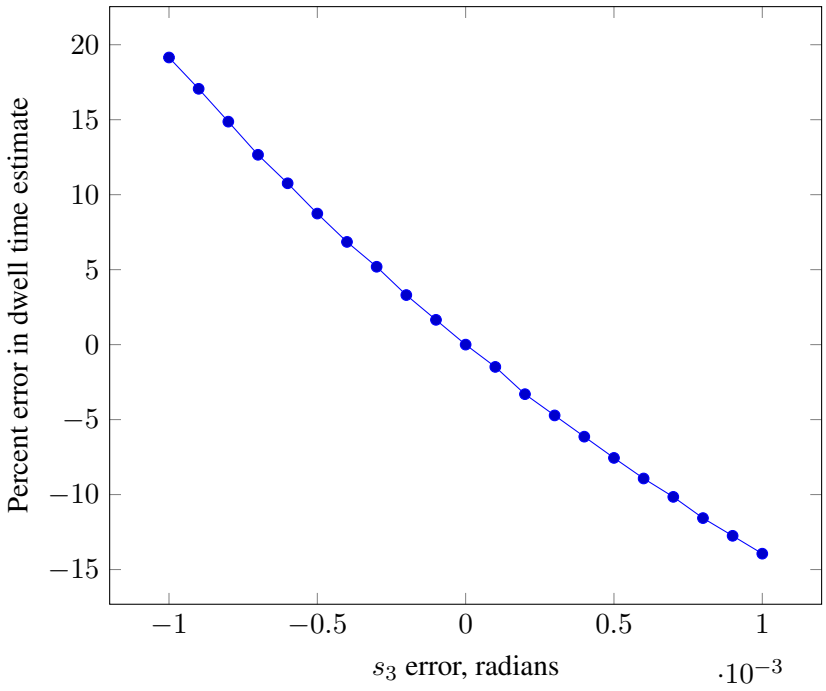

Figure 11: Percent error in dwell time from error in s_3 for $x_c = 0.001$

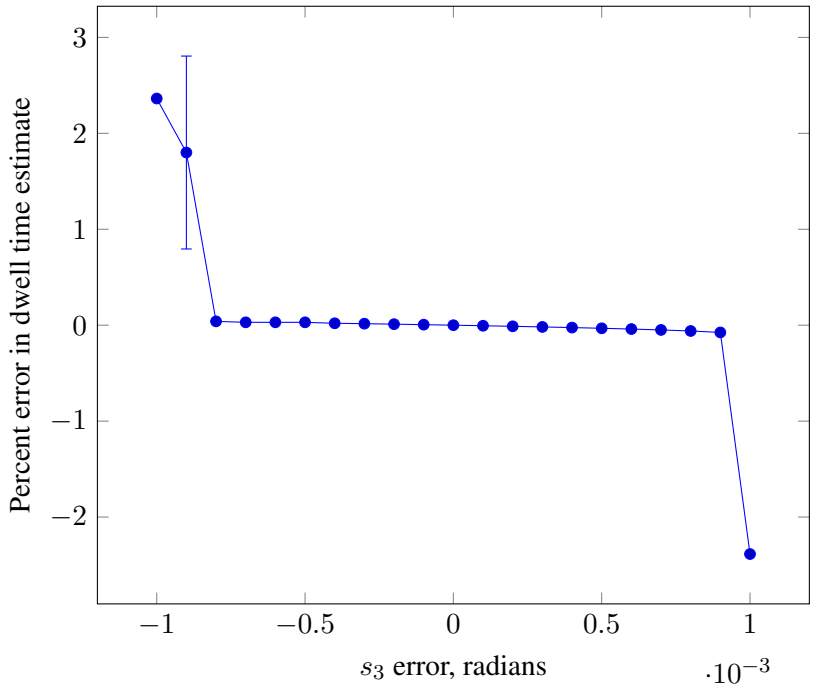

Figure 12: Percent error in dwell time from error in s_3 for $x_c = 0.01$

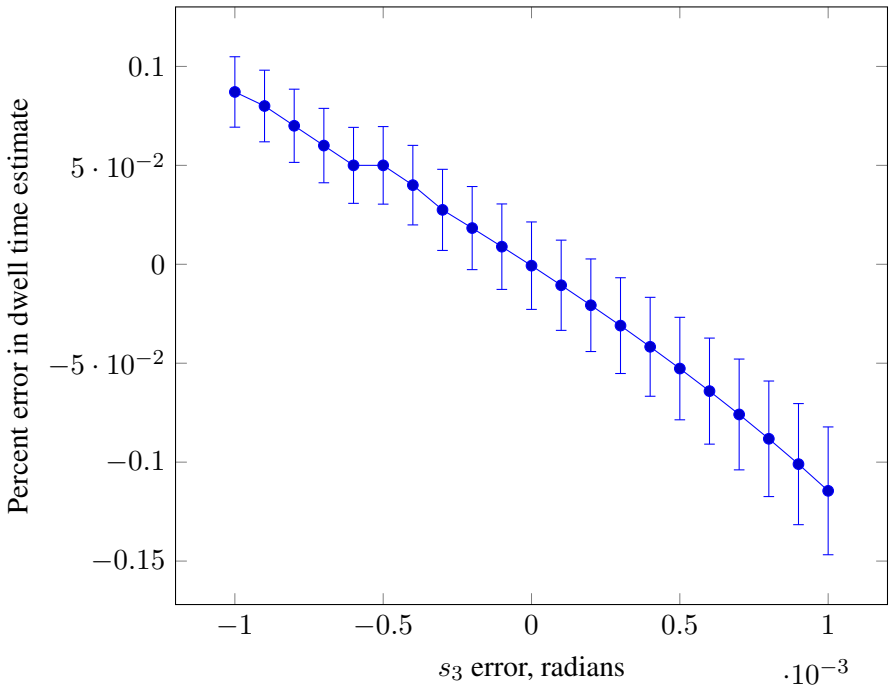

Figure 13: Percent error in dwell time from error in s_3 for $x_c = 0.1$

the range of s_2 errors; the standard deviation is so small it mostly does not show up on these plots except for fig. 13. The x_c computed from eq. (6) does not use s_3, however, it can also be computed from s_3 using a similar formula. Averaging the two results does not reduce the error significantly over using s_2 alone.

Note that while the percent errors seem rather large, particularly for the case of $x_c = 1 \times 10^{-4}$, these times are also very large, and it is unlikely that an orbit with dwell time 30 times too large will be regarded differently from the correct value, i.e., the orbits will both be presumed to by synchronized. Dwell time errors that are too low have a much smaller percentage error.

These uncertainties could arise because of clock variations, but a more likely reason is ambiguity of signal shape as the object passes through the sheet. If for example the leading edge of the detector signal is chosen as the reference time, a rotation of the secondary which changes the distance from the leading edge to the center of mass between sheet crossings, or other ambiguity in the signal, will introduce an error in the elapsed time measurement. At a secondary relative orbit scale of $\kappa = 1\,\mathrm{km}$, or $2\,\mathrm{km}$ difference between highest and lowest altitude, a one milliradian error corresponds to a $1\,\mathrm{m}$ ambiguity in the object detection.

CONCLUSION

Using a laser sheet and detector oriented perpendicular to the direction of travel on a host vehicle, a secondary object in the vicinity will be detected multiple times if the orbital periods (or semimajor axes) are close enough. From the three detections, it is possible to infer the dwell time, that is, the total time between first crossing and last crossing, with three simple formulas. The percentage error in this dwell time can be substantial based on a realistic uncertainty of the secondary's sheet crossing

time, but still allows a rough discrimination between objects with synchronized orbits. With two parallel sheets close together, it is possible to determine the complete motion in the orbital plane of the host.

REFERENCES

[1] Robert L. Scott and Alex A. Ellery. "Speckle Interferometry Tracking of On-Orbit Servicing in Geostationary Orbit". *Journal of Spacecraft and Rockets* 53.3 (Apr. 28, 2016), pp. 433–447. ISSN: 0022-4650. DOI: 10.2514/1.A33406. URL: https://arc.aiaa.org/doi/10.2514/1.A33406 (visited on 07/26/2018).

[2] Brook R. Sullivan, David L. Akin, and Gordon Roesler. "A Parametric Investigation of Satellite Servicing Requirements, Revenues and Options in Geostationary Orbit". In: *AIAA SPACE 2015 Conference and Exposition*. 0 vols. AIAA SPACE Forum. American Institute of Aeronautics and Astronautics, Aug. 28, 2015. DOI: 10.2514/6.2015-4477. URL: https://arc.aiaa.org/doi/10.2514/6.2015-4477 (visited on 08/07/2018).

[3] Christoph R. Englert, J. Timothy Bays, Kenneth D. Marr, Charles M. Brown, Andrew C. Nicholas, and Theodore T. Finne. "Optical orbital debris spotter". *Acta Astronautica* 104.1 (Nov. 2014), pp. 99–105. ISSN: 0094-5765. DOI: 10.1016/j.actaastro.2014.07.031. URL: http://www.sciencedirect.com/science/article/pii/S0094576514002872 (visited on 09/24/2014).

[4] D.C. Woffinden and D.K. Geller. "Observability Criteria for Angles-Only Navigation". *IEEE Transactions on Aerospace and Electronic Systems* 45.3 (July 2009), pp. 1194–1208. ISSN: 0018-9251. DOI: 10.1109/TAES.2009.5259193.

[5] Liam M. Healy and C. Glen Henshaw. "Trajectory Guidance Using Periodic Relative Orbital Motion". *Journal of Guidance, Control, and Dynamics* 38.9 (2015), pp. 1714–1724. ISSN: 0731-5090. DOI: 10.2514/1.G000945. URL: http://dx.doi.org/10.2514/1.G000945 (visited on 01/28/2016).